From Magic State Distillation to Dynamical Systems

Yunzhe Zheng^{1,2} and Dong E. Liu^{1,3}

Magic State Distillation (MSD) has been a research focus for fault-tolerant quantum computing due to the need for non-Clifford resource in gaining quantum advantage. Although many of the MSD protocols so far are based on stabilizer codes with transversal T gates, there exists quite several protocols that don't fall into this class. We propose a method to map MSD protocols to iterative dynamical systems under the framework of stabilizer reduction. With our mapping, we are able to analyze the performance of MSD protocols using techniques from dynamical systems theory, easily simulate the distillation process of input states under arbitrary noise model and visualize it using flow diagram. We apply our mapping to common MSD protocols for $|T\rangle$ state and find some interesting properties: The [[15, 1, 3]] code may distill states corresponding to \sqrt{T} gate and the [5,1,3] code can distill the magic state for corresponding to the T gate. Besides, we examine the exotic MSD protocols that may distill into other magic states proposed in [Eur. Phys. J. D 70, 55 (2016)] and identify the condition for distillable magic states. We also study new MSD protocols generated by concatenating different codes and numerically demonstrate that concatenation can generate MSD protocols with various magic states. By concatenating efficient codes with exotic codes, we can reduce the overhead of the exotic MSD protocols. We believe our proposed method will be a useful tool for simulating and visualization MSD protocols for canonical MSD protocols on $|T\rangle$ as well as other unexplored MSD protocols for other states.

1 Introduction

Practical quantum computation must operate at the logical level to achieve robustness to quantum noise [1, 2, 3]. To mitigate undesirable error propagation, logical operations are typically implemented transversally such that local errors will remain confined to their respective subsystems during the computation. However, a no-go theorem has shown that the transversal logical operations for any quantum error correcting (QEC) codes cannot achieve universal quantum computation [4, 5]. As Clifford operations are transversal in many common QEC codes [6, 7, 8], we thus need additional non-Clifford resources for universality. Magic states, or non-Clifford states, are therefore critical resources in universal fault-tolerant quantum computation.

Although magic states cannot be prepared fault-tolerantly in general, Magic State Distillation (MSD) [9] provides a general framework for obtaining high-fidelity magic states by consuming many copies of moderate-fidelity magic states. Provided that the input states meet certain fidelity requirement, we can distill the faulty magic states to approach ideal fidelity at the cost of a huge amount of raw faulty states. This distilltion process relies on Clifford operations, quantum measurements, and classical processing, all often assumed to be noiseless in the MSD setting due to their typical fault tolerance. Since the inception in 2005, the scope of MSD has been expanded by extensive research. For instance, we can distill into various kinds of magic states [10, 11] apart from the most popular magic states is the $|T\rangle = (|0\rangle + e^{i\pi/4} |1\rangle)/\sqrt{2}$ states that can be exploited to inject the T gate. In addition, recently there has been quite plenty of work that provides insight on lowering the overhead of MSD [12, 13, 14, 15, 16], which renders the MSD overhead γ for raw

¹Department of Physics, Tsinghua University, Beijing, 100084, China

²Department of Applied Physics, Yale University, New Haven, Connecticut, 06511, USA

³Frontier Science Center for Quantum Information, Beijing 100084, China

magic state cost appraoching to zero ¹. Furthermore, progress in experimental quantum hardware has also triggered interest in the practical application of magic states [3, 17, 18]. Numerous studies have sought to produce higher-quality magic states tailored to specific scenarios [19, 20, 21, 22].

Still, most of the previous works concentrate on MSD protocols based on stabilizer codes with transversal T gates. Due to the natural fault-tolerance of transversal gates, a [[n,k,d]] stabilizer code with transversal T gate will render a n-to-k MSD protocol for $|T\rangle$ state with order-d error suppression, i.e. the output error $\epsilon_o = O(\epsilon_i^d)$ scales asymptotically with the input error ϵ_i in the small error limitation. The raw input states are typically modeled as noisy versions of the ideal $|T\rangle$ state under depolarizing noise, $\rho(\epsilon) = (1-\epsilon)|T\rangle\langle T| + \epsilon Z|T\rangle\langle T|Z$, which relies on the fact that $|T\rangle$ is an eigenstate of the Hadamard-like gate $H_{xy} = \frac{X+Y}{\sqrt{2}}$, allowing input states to be symmetrized via H_{xy} -twirling without introducing additional noise [9]. However, for magic states higher in the Clifford hierarchy [11], the twirling process requires additional non-Clifford resources. As a result, the depolarizing noise model may no longer apply, and input states could exhibit biased noise. Moreover, many stabilizer codes that do not support transversal non-Clifford gates, such as the [[5,1,3]] code [9], the Steane code [23], and other small codes [10], can still facilitate magic state distillation. The analysis for these protocols cannot be directly regarded as a QEC process, and we need more delicate techniques to fully understand these MSD protocols.

To fill this gap, here we propose a method to map MSD protocols to dynamical systems. Our method can account for input states with biased noise, and can be used to analyze various MSD protocols conveniently. We can calculate the distillation efficiency by analyzing the Jacobian matrix and visualize MSD dynamics using flow diagram. Our method is based on the framework of stabilizer reduction [24], which is applicable to all MSD protocols characterized by stabilizer codes. We show the dynamical systems should all be rational functions defined in a multi-dimensional space. For single-qubit magic states, the dynamical system is defined within the Bloch sphere with coordinate (x, y, z). We demonstrate our mapping by visualizing common MSD protocols for $|T\rangle$ states. Surprisingly, we find the [[15, 1, 3]] protocol can distill into magic states corresponding to \sqrt{T} gates, though the trajectory is unstable and the error suppression is linear. The [[5,1,3]] protocol proposed to distill the state $|F\rangle\langle F|=(I+(X+Y+Z)/\sqrt{3})/2$ can distill the $|T\rangle$ as well. We then investigate the exotic MSD protocols numerically exemplified in Ref. [10], and show that the angle for distillable exotic magic states must be a solution for a single-variable polynomial equation. We also demonstrate convenient calculation for error suppression prefactor by Jacobian matrix. Finally, we consider the effect of code concatenation for MSD protocols. Assisted by our proposed mapping, we numerically show that concatenating two codes with different magic states can generate numerous protocols with new magic states. By concatenating efficient MSD protocols with exotic MSD protocols, we may reduce the overhead for exotic MSD protocols despite of the linear suppression. We believe our method will not only be a useful tool for visualizing MSD protocols, but also an important technique for discovering new interesting MSD protocols that distill into more versatile magic states.

2 Stabilizer Reduction

In MSD protocols, we typically begin with a stable supply of raw logical magic states that contain moderate noise. These raw magic states can be prepared through various methods, such as non-fault-tolerant unitary encoding circuits [25, 26] or measured-based state preparation factories [19, 20]. Based on a specific measurement pattern, a success post-selection heralds the prodution of a higher-fidelity magic state. By using the output states as input for subsequent rounds of distillation and applying the MSD protocols recursively, we can distill magic states to an arbitrary low error rate in the asymptotic limit, though which may require a large number of raw states.

There has been various MSD protocols since its proposal in 2005, and most of the known protocols can be fully characterized by stabilizer codes. For these protocols, we can describe them using a class of protocols called *Stabilizer Reduction* [24]:

Definition 1 (adopted from Ref. [24]) A n-to-k qubit stabilizer reduction (SR) for stabilizer code

¹The asymptotic cost for MSD with at least quadratic error suppression is given by $C \propto (\log \epsilon^{-1})^{\gamma}$, which can be understood as the number of raw states needed to produce a target state with error tolerance ϵ .

 \mathcal{Q} performs the following: (i) take an n-qubit input state ρ_{in} ; (ii) measure all stabilizer generators g_i for i=1,2...,(n-k); (iii) postselect on the measurement outcomes of error-detecting stabilizers with all +1, and record the measurement outcomes of the other non-error-detecting stabilizers to decide the final gauge correction \mathcal{C}_g ; (iii) Decode the post-measurement state onto k output qubits with the logical operators \bar{X}_i and Z_i for i=1,2,...k and gauge correction \mathcal{C}_g .

The effect of stabilizer reduction is projecting the input state ρ_{in} onto the codespace of \mathcal{Q} , and the success probability p_s is given by the overlap of the input state and codespace:

$$p_s = \text{Tr}[P_{\mathcal{Q}}\rho_{in}P_{\mathcal{Q}}] = \text{Tr}[P_{\mathcal{Q}}\rho_{in}], \tag{1}$$

where $P_{\mathcal{Q}}$ is the codespace projector for code \mathcal{Q} and we used the fact that $P_{\mathcal{Q}}^2 = P_{\mathcal{Q}}$. For MSD protocols that allow gauge correction, the overall success rate should be a multiply of p_s

$$p_{s,all} = 2^{n_g} p_s, \tag{2}$$

where n_g is the number of non-error-detecting stabilizer generators. An example of gauge stabilizers is all Z-type generators in the [[15,1,3]] code [9], as only Z errors can be presented in the input magic states if they are under Pauli noise channel², and Z-type generators cannot detect them. Without loss of generality, we ignore the gauge correction from now and only consider post-selection on all +1 outcome of stabilizer measurements.

The codespace projector $P_{\mathcal{Q}}$ is given by the product of $\bar{n} = n - k$ projectors associated with stabilizer generators g_i , and can be further expanded as a sum of $2^{\bar{n}}$ all stabilizer element s_i :

$$P_{\mathcal{Q}} = \prod_{i=1}^{\bar{n}} P_i = \prod_{i=1}^{\bar{n}} \frac{I + g_i}{2} = \frac{1}{2^{\bar{n}}} \sum_{i=1}^{2^{\bar{n}}} s_i.$$
 (3)

After successful projection, the post-measurement state is given by

$$\rho_p = P_{\mathcal{Q}}\rho_{in}P_{\mathcal{Q}}/p_s \propto P_{\mathcal{Q}}\rho_{in}P_{\mathcal{Q}}.\tag{4}$$

At this stage, ρ_p is still a *n*-qubit state lying on the logical codespace. For gate injection or next-level distillation, we need to decode the states out with logical operators \bar{X}_i and \bar{Z}_i . The output decoded states are given by

$$\rho_i^{out} = \rho(x_i^o, y_i^o, z_i^o) = \frac{1}{2} (I + x_i^o X + y_i^o Y + z_i^o Z)$$
 (5)

for i = 1, 2..k, with

$$\begin{cases} x_i^o = Tr[\rho_p \bar{X}_i] = Tr[P_{\mathcal{Q}} \rho_{in} \bar{X}_i]/p_s \\ y_i^o = Tr[\rho_p \bar{Y}_i] = Tr[P_{\mathcal{Q}} \rho_{in} \bar{Y}_i]/p_s \\ z_i^o = Tr[\rho_p \bar{Z}_i] = Tr[P_{\mathcal{Q}} \rho_{in} \bar{Z}_i]/p_s, \end{cases}$$
(6)

where we used the property that all logical Pauli operators should commute with the codespace projector. For convenience, we define

$$\begin{cases}
T_i^x \triangleq Tr[P_{\mathcal{Q}}\rho_{in}\bar{X}_i] \\
T_i^y \triangleq Tr[P_{\mathcal{Q}}\rho_{in}\bar{Y}_i] \\
T_i^z \triangleq Tr[P_{\mathcal{Q}}\rho_{in}\bar{Z}_i].
\end{cases}$$
(7)

Technically, the decoding can be implemented by using a decoder unitary operation $D_{\mathcal{Q}}$ composed of only Clifford gates and tracing out all ancilla qubits

$$\rho_i^{out} = \text{Tr}_{anc}[D_{\mathcal{Q}}\rho_p D_{\mathcal{Q}}^{\dagger}]. \tag{8}$$

The decoding circuit should effectively convert the logical states in codespace \mathcal{Q} back to physical states with ancilla qubits all in $|0\rangle$ (Fig. 1(a)). For any k-qubit logical state $|\bar{\psi}\rangle$, we have

$$D_{\mathcal{Q}} \left| \bar{\psi} \right\rangle = \left| \psi \right\rangle \otimes \left| 0 \right\rangle^{\otimes \bar{n}}. \tag{9}$$

²This is due to Pauli X and Y errors can be effectively regarded as coherent Z errors for $|T\rangle$.

The decomposed implementation of the decoder circuit can be found using Gottesmans's algorithm given the stabilizer description of \mathcal{Q} [27]. Besides, as we can propagate the stabilizer measurements after the decoder circuit, we can perform the decoder circuit directly on the input state and measure out every ancilla. The overall circuit implementation of a stabilizer reduction protocol is therefore given in Fig. 1(b). Notably, there is no need to encode the input state onto the codespace of \mathcal{Q} , and only decoding is required.

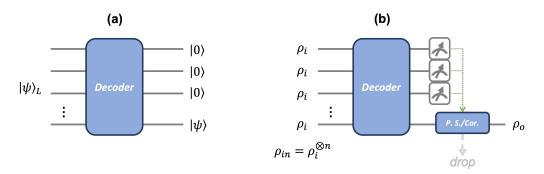


Figure 1: (a) Effect of the decoder operation. The decoder circuit transform the codespace of code $\mathcal Q$ to the trivial code with single-qubit stabilizer Z on each ancilla qubit. (b) Scheme for stabilizer reduction protocol characterized by stabilizer code $\mathcal Q$ when $\rho_{in}=\rho_i^{\otimes n}$. We prepare the tensor product of raw magic states as the input and apply a decoder circuit for $\mathcal Q$. We the measure the n-k ancilla qubits and post-select on the outcome of all +1. For some $\mathcal Q$ (e.g. [[15,1,3]] code), we only need to post-select on a subset of all stabilizer generators and can correct the state back by using the measurement outcome of the other generators.

3 Mapping to dynamical System

We might need multiple times of recursion in MSD to output distilled states with tolerable error rate, and it's a common practice to assume the input state to be a tensor product of identical single-qubit state, i.e. $\rho_{in} = \rho^{\otimes n}$. We now show that we can map the stabilizer reduction protocols into dynamical systems. Without loss of generality, we consider protocols that distill into single-qubit magic states. Any single-qubit quantum state can be represented by

$$\rho = \rho(x, y, z) = \frac{1}{2}(I + xX + yY + zZ),\tag{10}$$

where X, Y, Z are Pauli matrices and $x^2 + y^2 + z^2 \le 1$. x, y, z can be understood as the coordinate of the state within the Bloch sphere. Multi-qubit magic states can be represented with coordinates on a higher-dimensional space and will share the same framework as single-qubit states. Although the input state for MSD can be any form in general, we often assume they are the tensor product of the same states due to the recursion nature of the distillation process. In such case, we have:

Proposition 1 When $\rho_{in} = \rho(x, y, z)^{\otimes n}$, p_s, T_i^x, T_i^y, T_i^z are all polynomial of x, y, z with order no larger than n.

Proof. Let's show for p_s first. Combine Equation 1 and 3 and use $\rho_{in} = \rho^{\otimes n}$, we have

$$p_s = \frac{1}{2^{\bar{n}}} \sum_{j=1}^{2^{\bar{n}}} Tr[s_j \rho^{\otimes n}]. \tag{11}$$

Meanwhile, s_i is a *n*-qubit stabilizer operator and can be written as

$$s_j = (-1)^{\alpha_j} s_j^1 \otimes s_j^2 \dots \otimes s_j^n, \tag{12}$$

where $\alpha_j \in \{0,1\}$ and $s_j^l \in \{I,X,Y,Z\}$ for l=1,...n. As both the input states and the observable s_j are tensor product of independent single-qubit state (operator), we can make the following

simplification and calculate for each single-qubit subsystem

$$Tr[s_{j}\rho^{\otimes n}] = (-1)^{\alpha_{j}}Tr[\bigotimes_{k=1}^{n} s_{j}^{k}\rho]$$

$$= (-1)^{\alpha_{j}}\prod_{k=1}^{n}Tr[s_{j}^{k}\rho]$$

$$= (-1)^{\alpha_{j}}x_{j}^{w_{j}^{X}}y_{j}^{w_{j}^{Y}}z_{j}^{w_{j}^{Z}},$$

$$(13)$$

where w_j^X, w_j^Y, w_j^Z are separately the weight of X, Y, Z in stabilizer operator s_j . Therefore, p_s is a sum of polynomial terms with x, y, z:

$$p_s = \frac{1}{2^{\bar{n}}} \sum_{j=1}^{2^{\bar{n}}} (-1)^{\alpha_j} x^{w_j^X} y^{w_j^X} z^{w_j^Z}, \tag{14}$$

and the maximal order of p_s should be no larger than n as $w_j^X + w_j^Y + w_j^Z \le n$. Now the same conclusion is easily approachable for T_i^x, T_i^y, T_i^z . For example,

$$T_i^x = \frac{1}{2^{\bar{n}}} \sum_{j=1}^{2^{\bar{n}}} Tr[\bar{X}_i s_j \rho^{\otimes n}], \tag{15}$$

while $\bar{X}_i s_j$ is still a *n*-qubit Pauli operator. We therefore only need to substitute the s_j to $\bar{X}_i s_j$ in the calculation of p_s and count the Pauli weight for every $\bar{X}_i s_j$ operator. Therefore, we have

$$T_i^x = \frac{1}{2^{\bar{n}}} \sum_{i=1}^{2^{\bar{n}}} (-1)^{\alpha_j} x^{\tilde{w}_{i,j}^X} y^{\tilde{w}_{i,j}^Y} z^{\tilde{w}_{i,j}^Z}, \tag{16}$$

where $\tilde{w}_{i,j}^X, \tilde{w}_{i,j}^Y, \tilde{w}_{i,j}^Z$ are separately the weight of X, Y, Z in stabilizer operator $\bar{X}_i s_j$. The same conclusion also holds for T_i^y and T_i^z :

$$T_i^y = \frac{1}{2^{\bar{n}}} \sum_{j=1}^{2^{\bar{n}}} (-1)^{\alpha_j} x^{\bar{w}_{i,j}^X} y^{\bar{w}_{i,j}^Y} z^{\bar{w}_{i,j}^Z}$$

$$\tag{17}$$

$$T_i^z = \frac{1}{2^{\bar{n}}} \sum_{j=1}^{2^{\bar{n}}} (-1)^{\alpha_j} x^{\hat{w}_{i,j}^X} y^{\hat{w}_{i,j}^Y} z^{\hat{w}_{i,j}^Z}, \tag{18}$$

with $\bar{w}_{i,j}^X, \bar{w}_{i,j}^Y, \bar{w}_{i,j}^Z$ being the weight of X, Y, Z in stabilizer operator $\bar{Y}_i s_j$ and $\hat{w}_{i,j}^X, \hat{w}_{i,j}^Y, \hat{w}_{i,j}^Z$ being the weight of X, Y, Z in stabilizer operator $\bar{Z}_i s_j$. \square

The above proof also provides an explicit way to calculate p_s, T_i^x, T_i^y, T_i^z for a specific stabilizer code Q. Therefore, for each magic state distillation protocol for single-qubit magic states, we can map it to an iterative dynamical process on a three-dimensional space within the Bloch sphere:

Proposition 2 For stabilizer reduction protocols that distill into single-qubit magic states, the process can be mapped into a dynamical system within the three-dimensional Bloch sphere. $\rho_o = \mathcal{D}_{\mathcal{Q}}(\rho) \propto Tr_{anc}[D_{\mathcal{Q}}\bar{P}\rho^{\otimes n}\bar{P}D_{\mathcal{Q}}].$

For simplicity we now consider k = 1 case (single output). The output state in Equation 6 is given by

$$\begin{cases} x^{o} = Tr[\rho_{p}\bar{X}_{i}] = T_{x}(x, y, z)/p_{s}(x, y, z) \\ y^{o} = Tr[\rho_{p}\bar{Y}_{i}] = T_{y}(x, y, z)/p_{s}(x, y, z) \\ z^{o} = Tr[\rho_{p}\bar{Z}_{i}] = T_{z}(x, y, z)/p_{s}(x, y, z), \end{cases}$$
(19)

and we have a discrete map $(x, y, z) \xrightarrow{\mathcal{D}_{\mathcal{Q}}} (x^o, y^o, z^o)$ within the Bloch sphere and are able to derive its analytical form.

Now that we mapped the distillation protocols into dynamical system, we are able to gain several advantages from this mapping: First, We can easily find out all potential target states that a protocol might be able to distill into. This can be done by solving the fixed-point equations and finding every non-trivial fixed points, either analytically or numerically:

$$\begin{cases} x = T_x(x, y, z)/p_s(x, y, z) \\ y = T_y(x, y, z)/p_s(x, y, z) \\ z = T_z(x, y, z)/p_s(x, y, z) \\ x^2 + y^2 + z^2 = 1. \end{cases}$$
(20)

As all target magic states must be fixed points in the dynamical system, we can easily check all potential target states a protocol could distill into. Later we will show this also allows to account for some exotic magic states that distilled by small codes [10], and all the examples should be a solution of a single-variable polynomial equation. Second, we can obtain the distillation efficiency by analyzing the convergence rate of the fixed points. For example, we can use the Jacobian matrix around a given fixed point $\mathbf{x}^* = (x^*, y^*, z^*)$ to analysis its first order convergence of all direction. The Jacobian matrix is given by

$$J = \begin{bmatrix} \frac{\partial}{\partial x} \left(\frac{T_x}{p_s} \right) & \frac{\partial}{\partial y} \left(\frac{T_x}{p_s} \right) & \frac{\partial}{\partial z} \left(\frac{T_x}{p_s} \right) \\ \frac{\partial}{\partial x} \left(\frac{T_y}{p_s} \right) & \frac{\partial}{\partial y} \left(\frac{T_y}{p_s} \right) & \frac{\partial}{\partial z} \left(\frac{T_y}{p_s} \right) \\ \frac{\partial}{\partial x} \left(\frac{T_z}{p_s} \right) & \frac{\partial}{\partial y} \left(\frac{T_z}{p_s} \right) & \frac{\partial}{\partial z} \left(\frac{T_z}{p_s} \right) \end{bmatrix}_{|\boldsymbol{x}^*}$$
(21)

We can calculate the eigenvalue of the Jacobian matrix near a fixed point and judge the property of the fixed point. For discrete system, if $|\lambda_i| < 1$ for all the eigenvalue λ_i of J, then the fixed point is stable and there should exist a nearby convergence region. Furthermore, if they are all zero, we instantly know if the distillation protocols are of at least quadratic error suppression. The eigenvalues also correspond to the prefactor of the convergence speed in a given spatial direction. For higher order analysis, it would be more computationally efficient to determine a spatial direction and then calculate its directional derivative using the analytical description of the system. Furthermore, the dynamical system also offers the flexibility to consider a more generalized Pauli noise model for the input state. Many previous analyses have focused on depolarized input magic states, which are compatible with twirling operations that symmetrize errors; however, this approach may not be suitable for protocols that distill magic states other than the $|T\rangle$ states. Our framework therefore enables the analysis of input magic states with biased logical noise, which may be suitable for investigating various hardware-specific protocols.

We may further reduce the three-dimensional dynamical system to a two-dimensional system by setting z=0. The target magic states for most MSD protocols can also be chosen as $|\theta\rangle=(|0\rangle+e^{i\theta}|1\rangle)/\sqrt{2}$ such that they lie on the xy plane. When we prepare the raw logical magic states, as the QEC process will ultimately eliminate coherent logical errors [28], we might assume that the raw states are the ideal states under logically decoherent Pauli noise. As decoherent noise cannot create the z component of $|\theta\rangle$, we can make sure that our raw input states are also in the xy plane. Furthermore, we provide the condition for a stabilizer code such that z=0 can be a fixed plane during the MSD process:

Proposition 3 For a stabilizer code Q, z=0 is a fixed plane in the mapped dynamical system if $s_j * \bar{Z}_i$ explicitly contains Pauli Z operators for every logical operator $\bar{Z}_i(i=1,...,k)$ and every stabilizer element $s_j(j=1,...,2^{\bar{n}})$.

If each $s_j * \bar{Z}_i$ contains at least one Pauli Z, then

$$T_i^z(x, y, z) = z * \tilde{T}_i^z(x, y, z)$$
(22)

Therefore, $T_i^z(x, y, 0) = 0$, which means z = 0 is a fixed plane for the system. This condition is satisfied by most known protocols that we have examined and we conjecture it to be generally true for any stabilizer codes by properly choosing the logical Z operators without modifying the stabilizer groups.

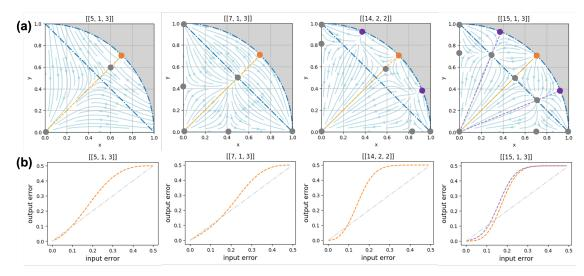


Figure 2: (a) flow diagram in the z=0 plane for [[5,1,3]], [[7,1,3]], [[14,2,2]] and [[15,1,3]] protocols. All these protocols can distill into the $|T\rangle$ states (yellow dot). The [[15,1,3]] can also distill the $|\pi/8\rangle$ and $|3\pi/8\rangle$ states (purple dot). All trivial fixed points are denoted as grey dots. (b) Input-output error relation for input state under depolarizing noise for each protocol, calculated using the analytical description of the dynamical systems. The plots for the [[7,1,3]] and [[15,1,3]] protocol distilling the $|T\rangle$ states match the previous results in [9,23], which is obtained under the specific code setting.

As an initial exploration of our mapping, we simulated the MSD protocols based on the [[5,1,3]] code [9], [[7,1,3]] Steane code [23], the [[14,2,2]] tri-orthogonal code [29] and [[15,1,3]] quantum Reed-Muller code [9] in Fig. 2. We derive the analytical description of the dynamical system for the given MSD protocols using Eqs. 14, 16, 17, and 18. Additionally, we analyze the reduced dynamical system by constraining z=0, as outlined in Prop. 3. The analytical description of the dynamical system for the specific codes can be found in Appendix C. Importantly, although all these MSD protocols can distill into the $|T\rangle$ states, only the [[14,2,2]] and [[15,1,3]] admit transversal implementation of the T gates. The order of error suppression for both [[5,1,3]] and [[7,1,3]] is just linear.

In Fig. 2(a), we plot the flow diagram of the dynamical system on the x-y cross section of Bloch sphere for z=0. This allows us to instantly visualize all fixed points and dynamics of the MSD protocols. We also plotted the output error rate versus input error rate for input state under depolarizing noise in Fig. 2(b), which matches the numerical result from the previous work [9, 23]. Surprisingly, we found out that both the [[15, 1, 3]] codes and [[14, 2, 2]] codes admit $|\pi/8\rangle$ as well as the $|3\pi/8\rangle$ as their fixed points, and [[15, 1, 3]] codes can distill into these magic states by choosing the input states exactly as the depolarized magic states (on the purple dashed line). However, the distillation dynamics is unstable and any perturbation will lead a different output states asymptotically, and the convergence rate is linear. Besides, the Steane codes distilling the $|T\rangle$ states is also unstable and fragile to perturbation. However, this might be circumvent by Hadamard twirling [9, 23], which allows us to engineer the input state to the form of depolarized $|T\rangle$ states on the yellow dashed line. We also find [[5, 1, 3]] code can distill into the $|T\rangle$ state, although it is proposed to distill the magic state $\rho_F = (I + (X + Y + Z)/\sqrt{3})/2$.

Within this dynamical system, we can also obtain the asymptotic convergence rate as well as the prefactor. For instance, we can calculate the Jacobian matrix for the Steane code at $x=y=1/\sqrt{2}$ based on the analytical form of the system (Appendix C),

$$J_* = \frac{1}{9} \begin{bmatrix} 14 & -7 \\ -7 & 14 \end{bmatrix}. \tag{23}$$

 J_* has two eigenvalues: 7/9 for eigenvector $\begin{bmatrix} 1 & 1 \end{bmatrix}^T$ and 7/3 for eigenvector $\begin{bmatrix} -1 & 1 \end{bmatrix}^T$. This first (radial) eigenvalue matches the prefactor for linear convergence in [23], which shows that the convergence for Steane code is $\epsilon' = \frac{7}{9}\epsilon$ for input state suffering depolarizing noise. The other value is larger than 1, which denotes that the fixed point is not stable along the tangent direction.

4 Analyzing exotic MSD protocols

In the paper by M. Howard and H. Dawkins [10], they highlight several small stabilizer codes that could be used to distill exotic magic states other than the canonical $|T\rangle$ states. However, they just provided numerical evidence for these protocols, and the fundamental reason behind these exotic distillable states is still unclear. Within our mapping framework, we now show that we can analyze these protocols in a convenient way and understand these exotic magic states. The smallest stabilizer code that are able to distill magic states is a [[3,1,1]] code with stabilizer generator $\{XZI,ZXX\}$ and $X_L=IZZ,Z_L=IIX$. Although this code cannot even detect a single error, it can be used to distill into the state that is equivalent to $|\theta\rangle=(|0\rangle+e^{i\theta}|1\rangle)/\sqrt{2}$ with $\theta=\arctan\sqrt{(\sqrt{5}-1)/2}$, with linear error supporession. However, it's not clear why this code could distill into this particular state. Applying our framework to this code, we can obtain the reduced dynamical system as 3

$$\begin{cases} x' = \frac{xz + z^2}{1 + xz + x^2z} \\ z' = \frac{x + xz + x^2z}{1 + xz + x^2z}. \end{cases}$$
 (24)

As we mentioned earlier, any distillable states must be a solution to the fixed point equation for Eq. 24. We can reduce the equation as

$$x^2 + x^2z + x^3z = xz^2 + z^3 (25)$$

Assume $x = \sin \theta$ and $z = \cos \theta$ and define $t = \tan(\theta/2)$, we have $x = \frac{2t}{1+t^2}$, $z = \frac{1-t^2}{1+t^2}$

$$t^{8} - 2t^{7} - 2t^{6} - 6t^{5} + 8t^{4} + 10t^{3} + 10t^{2} - 2t - 1 = 0$$
(26)

Which is equivalent to

$$(t^4 - 4t - 1)(t^4 - 2t^3 - 2t^2 - 2t + 1) = 0 (27)$$

solve it out, we have $t=(1+\sqrt{5}\pm\sqrt{2(1+\sqrt{5})})/2$ or $t=(1\pm\sqrt{2\sqrt{2}-1})/\sqrt{2}$. The solution corresponds to $\theta=\arctan\left(\frac{2t}{1-t^2}\right)$. By restricting $\theta>0$, the only solution is $t=(1+\sqrt{5}-\sqrt{2(1+\sqrt{5})})/2$, which exactly corresponds to $\theta=\arctan\sqrt{\frac{\sqrt{5}-1}{2}}$.

For all magic states, because the MSD protocols should fulfill "good-in, good-out" property, being fixed points for the dynamical systems is a necessary condition to be distillable. As we can always set $x = \sin \theta, z = \cos \theta$ in the dynamical system, combined with Prop. 1 we instantly have the following conclusion:

Proposition 4 For any exotic magic states distillable with stabilizer codes \mathcal{Q} formed as $|\theta\rangle = (|0\rangle + e^{i\theta} |1\rangle)/\sqrt{2}$, θ must be $\arctan\left(\frac{2t}{1-t^2}\right)$ where t is a solution for a single-variable polynomial equation associated with the stabilizer codes $f_{\mathcal{Q}}(t) = 0$.

We also conjecture that there is some structure hidden in the coefficient of the high-order polynomial equation $f_{\mathcal{Q}}(t)$. With Prop. 4, we are able to find out the corresponding f(t) for all the numerical examples given there. As another two examples, we consider the [[4,1,1]] code in the Fig. 3(b) and the [[6,1,2]] in Fig. 6(c) from [10]. For the four-qubit code, its stabilizer group is generated by $\{XZII, ZXZX, IZXI\}$ with logical operator $Z_L = IIIX, X_L = IZIZ$. This four-qubit code cannot detect a single error as well for its Z_L being single-weight. By doing the same routine for the three-qubit code, we are able to find out that the polynomial equation to be

$$t^5 - t^4 + 6t^3 + 2t^2 + t - 1 = 0 (28)$$

This equation doesn't have radical solution, but we are able to numerically solve it to be $t \approx 0.38296$, which corresponds to $\theta \approx 0.73146$. This matches the numerical result provided in the paper for $x = \sin \theta \approx 0.66796$ and $z = \cos \theta \approx 0.7442$.

³In the original paper they considered the xz plane. To coordinate with their convention, we reduced the dynamical system for y=0.

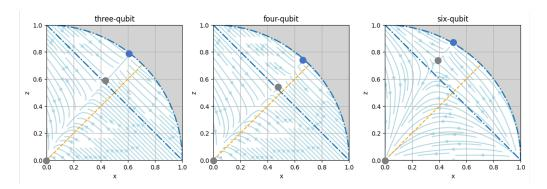


Figure 3: Flow diagram in the y=0 plane for the three small codes discussed in Sec 4: [[3,1,1]] code, [[4,1,1]] code and [[6,1,2]] code. The blue dots correspond to the target magic states, and the grey dots are the trivial fixed points. The yellow dashed line corresponds to the x=z for reference.

We can also calculate the asymptotic convergence rate by calculate the Jacobian matrix at the fixed point. The Jacobian matrix at the fixed point $x = \sin \theta_*, z = \cos \theta_*$ can be numerically evaluated:

$$J_{|\theta_*} \approx \begin{bmatrix} -0.05673 & 0.80093\\ 0.82913 & 0.14814 \end{bmatrix}$$
 (29)

For this matrix, we have eigenvalue $\lambda_1 \approx 0.867$ and $\lambda_2 \approx -0.775$, with corresponding eigenvector being $[0.867, 1]^T$ and $[-1.114, 1]^T$. As both the absolute value of both eigenvalues are smaller than one, we again confirm that the fixed point is stable.

For the six-qubit code, it could distill into the $|\pi/6\rangle$ magic states. From the fixed point equation, we can get the expression of the equation f(t):

$$(t-1)^{3}(t+1)^{5}(t^{2}-4t-1)(t^{2}-4t+1) = 0$$
(30)

One of the root is $t=2-\sqrt{3}$, which corresponds to $\theta=\pi/6$. The Jacobian matrix is given by

$$J = \begin{bmatrix} 38 - 22\sqrt{3} & -48 + 28\sqrt{3} \\ -62 + 36\sqrt{3} & 118 - 68\sqrt{3}, \end{bmatrix}$$
 (31)

with eigenvalue $\lambda_1 = 2(5 - 3\sqrt{3}) \approx -0.3923$ with eigenvector $[-\sqrt{3}, 1]^T$ and $\lambda_2 = 2(73 - 42\sqrt{3}) \approx 0.5077$ with eigenvector $[\frac{2+4\sqrt{3}}{11}, 1]^T$. The minus eigenvalue corresponds to the direction tangent to the Bloch sphere, while the radial eigenvector has a small angle shift.

5 MSD with code concatenation

As we map MSD protocols to dynamical system, MSD protocols with code concatenation are also mapped to nested dynamical systems. If we have two MSD protocols Q_A and Q_B with mapped system \mathcal{D}_A and \mathcal{D}_B , then the MSD protocol described by concatenated codes Q_A (inner) and Q_B (outer) is mapped to $\mathcal{D}_B \circ \mathcal{D}_A$. The concatenation can be done recursively, which allows to create more MSD protocols from some simple base protocols.

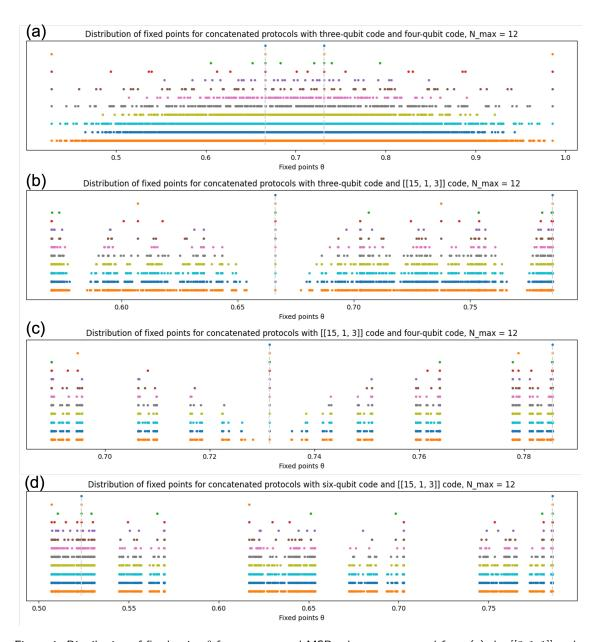


Figure 4: Distribution of fixed point θ for concatenated MSD schemes, generated from (a) the [[3,1,1]] code and the [[4,1,1]] code (b) the [[3,1,1]] code and the [[15,1,3]] code (c) the [[4,1,1]] code and the [[15,1,3]] code (d) the [[6,1,2]] code and the [[15,1,3]] code. The level of concatenation increased from 1 to 12 from upper to lower row. The θ for the two base codes are highlighted with grey dashed lines.

5.1 More exotic magic states

By concatenating codes that distill into different magic states, we can create MSD protocols that distill into new magic states. Take the [[3,1,1]] and [[4,1,1]] code we mentioned in the last section as the base codes, we can generate various MSD protocols for new magic states with θ ranging from 0.428 to 0.985 if we range the concatenation level from 1 to 12 as shown in Fig. 4(a). In the uppermost row, we only consider the [[3,1,1]] protocol and [[4,1,1]] protocol themselves. By allowing more concatenation level, we can generate a set of MSD protocols with more various target magic states. Notably, the range of generated fixed point angle can be larger than the range of the angles for the two base codes. However, our further numerical test shows that we may not be able to generate dense set for the fixed point angle by only concatenating two codes. Besides, for small codes concatenated with [[15,1,3]] codes, the distribution of the fixed points exhibit fractal

behavior (Fig. 4(b-d)), which is typically a result of iterative systems and has also been discussed in [30, 31]. We discuss the fractal property in detail in Appendix D.

5.2 Higher distillation efficiency

Although all the known exotic MSD protocols only allow linear error suppression and have unsatisfying cost scaling compared with canonical protocols, we may reduce the overhead by concatenating exotic MSD protocols with canonical protocols with good cost scaling. For example, we may concatenate the [[4,1,1]] code with the [[15,1,3]] code that allows for order-3 error suppression for multiple levels. We may greatly reduce the prefactor for linear convergence as shown in Fig. 5(a), although we cannot upgrade the convergence order to more than linear asymptotically. We further estimate the cost for obtaining exotic magic states from our concatenated protocols and the [[15,1,3]] protocol together with gate synthesis. The cost for a n-to-k MSD protocol with linear error suppression $\epsilon_{out} = k' \epsilon_{in}$ and success probability p_s is given by

$$C = \left(\frac{\epsilon_{in}}{\epsilon_{tar}}\right)^{\beta}, \quad \beta = \frac{\log 1/k'}{\log n/kp_s}$$
 (32)

In comparison, the cost for [[15, 1, 3]] protocol is $\log^{\gamma}(1/\epsilon_{tar})$ with $\gamma = \log_3 15 \approx 2.465$. For the optimal gate synthesis based on T gates, the cost just scales with $\log(1/\epsilon_{tar})$ linearly with a constant prefactor [32]. We plot the scaling of cost in Fig. 5(b). Although all of the concatenated exotic MSD protocols cannot outperform the canonical protocol asymptotically, we may still find practical error regime where our protocols may render advantage.

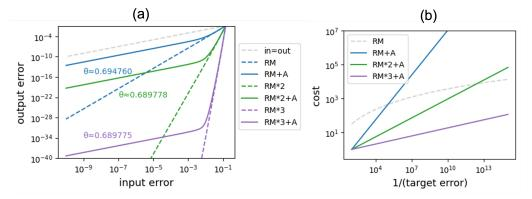


Figure 5: (a) input-output error relation for different concatenated MSD schemes, with $\epsilon_{in}=0.01$. 'RM' stands for the [[15,1,3]] protocols and 'A' stands for the [[4,1,1]] protocol. The θ for target magic states is shown near the curve. Although concatenation cannot improve the convergence order, it can significantly increase the prefactor for linear convergence. (b) Estimation of raw state cost for distillation. For the 'RM' protocol, we also considered the overhead for gate synthesis. With more concatenation with the

6 Summary and open questions

In this work, we proposed a method that maps MSD protocols to dynamical systems using the framework of stabilizer reduction. We showed it to be a convenient way to visualize the process of MSD under iteration, and demonstrate efficiency analysis for common MSD protocols. Besides, we applied our method to those exotic MSD protocols proposed in [10]. We are able to have a further understanding on the condition of distillable exotic magic states and our method can also be used to analyze these procotols in an analytical way. Furthermore, we numerically studied the potential of concatenated MSD schemes using our method. We show that we might discover MSD protocols that distill into various exotic magic states, and the overhead due to linear error suppression can be reduced by further concatenation with efficient MSD protocols.

However, we have to emphasize that MSD protocols still require more understanding, especially for these protocols not based on transversal T gates. Here are some open questions that are worth more effort in our opinion:

- Is there any fundamental limitation for a magic state to be distillable? Given an arbitrary angle θ and arbitrary error tolerance ϵ , can we construct a MSD protocol that distill $|\theta'\rangle$ with $|\theta \theta'| < \epsilon$? If so, gate synthesis might no longer be necessary, and we can always distill into the magic states corresponding to the $R_Z(\theta)$ gates we need.
- Can we find exotic MSD protocols with at least quadratic error suppression? By far all exotic MSD protocols we know only suppress error linearly. If we can improve it to at least quadratic, then the overhead can be reduced exponentially.
- How can we engineer MSD protocols such that it can distill into a given $|\theta'\rangle$? We have show concatenation has the potential to generate MSD protocols for new exotic magic states. How should we play around it to answer the first question? How many codes we may need, and what's the distribution of all distillable θ if we restrict our system size to a finite value?

We hope this work could pave the way for more versatile MSD protocols and deepen the common understanding of the fundamental principle of MSD protocols.

Code availability

The code used to produce the figures in this work can be found in here.

Acknowledgment

We thank Yuanchen Zhao and Johannes Borregaard for insightful discussion and Mark Howard for kind encouragement. We thank Pei-Kai Tsai for valuable comments on the manuscript. This work was supported by National Natural Science Foundation of China (Grants No. 92365111) and Beijing Natural Science Foundation (No. Z220002)

References

- [1] Google Quantum AI. "Quantum error correction below the surface code threshold" (2024). arXiv:2408.13687.
- [2] Hengyun Zhou, Chen Zhao, Madelyn Cain, Dolev Bluvstein, Casey Duckering, Hong-Ye Hu, Sheng-Tao Wang, Aleksander Kubica, and Mikhail D. Lukin. "Algorithmic Fault Tolerance for Fast Quantum Computing" (2024). arXiv:2406.17653.
- [3] Riddhi S. Gupta, Neereja Sundaresan, Thomas Alexander, Christopher J. Wood, Seth T. Merkel, Michael B. Healy, Marius Hillenbrand, Tomas Jochym-O'Connor, James R. Wootton, Theodore J. Yoder, Andrew W. Cross, Maika Takita, and Benjamin J. Brown. "Encoding a magic state with beyond break-even fidelity". Nature 625, 259–263 (2024).
- [4] Bryan Eastin and Emanuel Knill. "Restrictions on Transversal Encoded Quantum Gate Sets". Physical Review Letters 102, 110502 (2009).
- [5] Bei Zeng, Andrew Cross, and Isaac L. Chuang. "Transversality versus Universality for Additive Quantum Codes" (2007). arXiv:0706.1382.
- [6] Andrew Steane. "Multiple Particle Interference and Quantum Error Correction". Proceedings of the Royal Society of London. Series A: Mathematical, Physical and Engineering Sciences 452, 2551–2577 (1996). arXiv:quant-ph/9601029.
- [7] Austin G. Fowler. "Two-dimensional color-code quantum computation". Physical Review A 83, 042310 (2011).
- [8] Austin G. Fowler, Matteo Mariantoni, John M. Martinis, and Andrew N. Cleland. "Surface codes: Towards practical large-scale quantum computation". Physical Review A 86, 032324 (2012).
- [9] Sergey Bravyi and Alexei Kitaev. "Universal quantum computation with ideal Clifford gates and noisy ancillas". Physical Review A 71, 022316 (2005).

- [10] Mark Howard and Hillary Dawkins. "Small codes for magic state distillation". The European Physical Journal D 70, 55 (2016).
- [11] Guillaume Duclos-Cianci and Krysta M. Svore. "Distillation of nonstabilizer states for universal quantum computation". Phys. Rev. A 88, 042325 (2013).
- [12] Matthew B. Hastings and Jeongwan Haah. "Distillation with Sublogarithmic Overhead". Physical Review Letters 120, 050504 (2018).
- [13] Anirudh Krishna and Jean-Pierre Tillich. "Towards Low Overhead Magic State Distillation". Physical Review Letters **123**, 070507 (2019).
- [14] Adam Wills, Min-Hsiu Hsieh, and Hayata Yamasaki. "Constant-Overhead Magic State Distillation" (2024). arXiv:2408.07764.
- [15] Quynh T. Nguyen. "Good binary quantum codes with transversal CCZ gate" (2024). arXiv:2408.10140.
- [16] Louis Golowich and Venkatesan Guruswami. "Asymptotically Good Quantum Codes with Transversal Non-Clifford Gates" (2024). arXiv:2408.09254.
- [17] Seok-Hyung Lee, Felix Thomsen, Nicholas Fazio, Benjamin J. Brown, and Stephen D. Bartlett. "Low-overhead magic state distillation with color codes" (2024). arXiv:2409.07707.
- [18] Lucas Daguerre and Isaac H. Kim. "Code switching revisited: Low-overhead magic state preparation using color codes" (2024). arXiv:2410.07327.
- [19] Tomohiro Itogawa, Yugo Takada, Yutaka Hirano, and Keisuke Fujii. "Even more efficient magic state distillation by zero-level distillation" (2024). arXiv:2403.03991.
- [20] Christopher Chamberland and Andrew W. Cross. "Fault-tolerant magic state preparation with flag qubits". Quantum 3, 143 (2019).
- [21] Craig Gidney, Noah Shutty, and Cody Jones. "Magic state cultivation: growing t states as cheap as cnot gates" (2024). arXiv:2409.17595.
- [22] Hayato Goto. "Minimizing resource overheads for fault-tolerant preparation of encoded states of the steane code". Scientific reports 6, 19578 (2016).
- [23] Ben W. Reichardt. "Quantum Universality from Magic States Distillation Applied to CSS Codes". Quantum Information Processing 4, 251–264 (2005).
- [24] Earl T. Campbell and Dan E. Browne. "On the Structure of Protocols for Magic State Distillation" (2009). arXiv:0908.0838.
- [25] Oscar Higgott, Matthew Wilson, James Hefford, James Dborin, Farhan Hanif, Simon Burton, and Dan E. Browne. "Optimal local unitary encoding circuits for the surface code". Quantum 5, 517 (2021).
- [26] Ying Li. "A magic state's fidelity can be superior to the operations that created it". New Journal of Physics 17, 023037 (2015).
- [27] Daniel Gottesman. "Stabilizer Codes and Quantum Error Correction" (1997). arXiv:quant-ph/9705052.
- [28] Stefanie J. Beale, Joel J. Wallman, Mauricio Gutiérrez, Kenneth R. Brown, and Raymond Laflamme. "Quantum error correction decoheres noise". Phys. Rev. Lett. 121, 190501 (2018).
- [29] Sergey Bravyi and Jeongwan Haah. "Magic-state distillation with low overhead". Physical Review A 86, 052329 (2012).
- [30] Patrick Rall. "Fractal Properties of Magic State Distillation" (2017). arXiv:1708.09256.
- [31] Patrick Rall. "Signed quantum weight enumerators characterize qubit magic state distillation" (2017). arXiv:1702.06990.
- [32] Vadym Kliuchnikov, Dmitri Maslov, and Michele Mosca. "Practical approximation of single-qubit unitaries by single-qubit quantum clifford and t circuits". IEEE Transactions on Computers 65, 161–172 (2016).
- [33] "Wikipedia for box counting". url: https://en.wikipedia.org/wiki/Box_counting.

Algorithm for mapping stabilizer codes

We here describe the implementation of our mapping algorithm. The input should be a list of stabilizer generators generator_set, and a list of logical operators logical_operators. The output will be a list of polynomial function used for describing $p_s(x,y,z)$, $T_i^{x,y,z}(x,y,z)$.

- 1. Calculate all elements in the full stabilizer group from the generator_set, store all the elements as stabilizer_set. This can be down by take all possible combination of generators and multiply the chosen generators together.
- 2. Calculate p_s by counting the number of X, Y, Z for each element in stabilizer_set. Initialize a dictionary counter for counter_ps in empty, then for each element s_i , counter the weight of X, Y, Z as w_x, w_y, w_z . If (w_x, w_y, w_z) is already in counter_ps, add the value by one. Else, add the element (w_x, w_y, w_z) and initialize the value to one. Convert the counter_ps to p_s by treating each element in counter_ps as a polynomial term and the corresponding value as the coefficient.
- 3. For each logical qubit with logical X_i and Z_i , calculate $T_i^{x,y,z}(x,y,z)$ by similarly counting the weight for X, Y, Z in operator $s_j * X_i, s_j * Y_i, s_j * Z_i$. For example for T_i^x This can be done by generating Xstabilizer_set through multiplying X_i with stabilizer_set, and generating counter_xi by counting Pauli weights. Repeat this for T_i^y and T_i^z .
- 4. Repeat Step 3 for all logical qubits.

Description of [[15, 1, 3]] and [[14, 2, 2]] codes В

Both the [[15,1,3]] [9] and [[14,2,2]] [29] codes have logical transversal T gates and therefore can be used as MSD protocol to distill the T states. We give their stabilizer description here as they are practical small examples to work with.

The [[15,1,3]] code has 10 Z-type stabilizers and 4 X-type stabilizers. It's parity check matrix is given by

Notably, $H_Z = [H_X, H_Z']^T$. The logical operator is respectively $X_L = X^{\otimes 15}, Z_L = Z^{\otimes 15}$.

The [[14, 2, 2]] code has 9 Z-type stabilizers and 3 X-type stabilizers. It's parity check matrix is given by

where we used the sparse representation for H_Z by writing down the index of non-zero elements, e.g. the first row means $Z_2Z_3Z_4Z_5$. The logical operators are respectively $X_{L,1} = XXXXXXXIIIIIIII, Z_{L,1} = ZZZZZZZIIIIIIII,$ and $X_{L,2} = IIIIIIIXXXXXXXX, Z_{L,2} = IIIIIIIZZZZZZZZ$.

C Analytical form of dynamical systems

We give the analytical description of the reduced (z = 0) dynamical system for common codes that produced the Fig. 2. For the [[15, 1, 3]] code, we have

$$\begin{cases} x' = D_x(x,y) = \frac{x^{15} + 105x^{11}y^4 - 280x^9y^6 + 435x^7y^8 + 15x^7 - 168x^5y^{10} + 35x^3y^{12} + 105x^3y^4}{15x^8 + 15y^8 + 210x^4y^4 + 1} \\ y' = D_y(x,y) = \frac{y^{15} + 105y^{11}x^4 - 280y^9x^6 + 435y^7x^8 + 15y^7 - 168y^5x^{10} + 35y^3x^{12} + 105y^3x^4}{15x^8 + 15y^8 + 210x^4y^4 + 1} \end{cases}$$

For the [[14, 2, 2]] codes, the two output states share the same dynamical system:

$$\begin{cases} x' = D_x(x,y) = \frac{8x^7 + 56x^3y^4}{7x^8 + 98x^4y^4 + 7y^8 + 1} \\ y' = D_y(x,y) = \frac{8y^7 + 56y^3x^4}{7x^8 + 98x^4y^4 + 7y^8 + 1} \end{cases}$$
(36)

For the Steane code,

$$\begin{cases} x' = D_x(x,y) = \frac{x^7 + 7x^3y^4 + 7x^3}{7x^4 + 7y^4 + 1} \\ y' = D_y(x,y) = \frac{y^7 + 7y^3x^4 + 7y^3}{7x^4 + 7y^4 + 1}. \end{cases}$$
(37)

For the [[5, 1, 3]] code,

$$\begin{cases} x' = D_x(x,y) = \frac{5xy^2 - x^5}{5x^2y^2 + 1} \\ y' = D_y(x,y) = \frac{5x^2y - y^5}{5x^2y^2 + 1} \end{cases}$$
(38)

For the four-qubit code,

$$\begin{cases} x' = \frac{x^2 z^2 + 2xz + z^2}{x^2 z^2 + x^2 + 2xz + 1} \\ z' = \frac{x^3 + 2x^2 z + xz^2 + x}{x^2 z^2 + x^2 + 2xz + 1} \end{cases}$$
(39)

For the six-qubit code,

$$\begin{cases} x' = \frac{2x^4 + 2x^3 - 2x^2z^4 + 2xz^3 + z^4}{x^4 + 2x^3 + 4x^2z^3 + 2xz^3 + 1} \\ z' = \frac{x^5z - x^3z^3 + 2x^2z^2 + 2x^2z + xz^3 + 2xz^2 + xz}{x^4 + 2x^3 + 4x^2z^3 + 2xz^3 + 1} \end{cases}$$
(40)

D Fractal property of fixed point distribution

To verify the distribution of fixed points from concatenated protocols might exhibit fractal property, we exploit the box counting method [33] to numerically calculate the fractal dimension. We normalize the fixed point in range [0,1], vary the length of boxes ϵ , and calculate the number of boxes needed to cover all fixed points $N(\epsilon)$. The fractal dimension is given by

$$F_d = \lim_{\epsilon \to 0} |\log N(\epsilon) / \log \epsilon|$$

. Notice that we are unable to concatenate for arbitrary level to obtain the full distribution of fixed points, we have to truncate ϵ before the log N saturating. We therefore numerically calculate the fractal dimension by taking a linear fit for the linear part as in Fig. 6. We find out the fractal

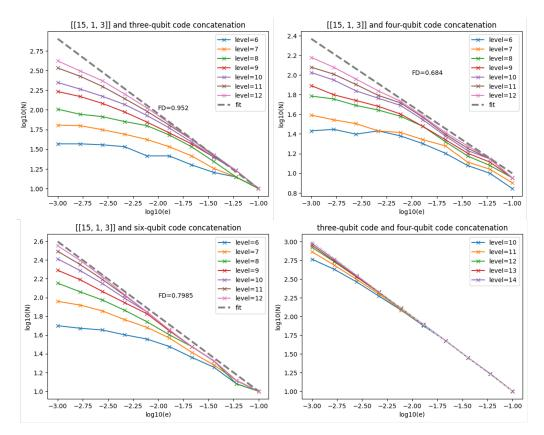


Figure 6: Fractal dimension of the fixed point distribution for concatenated protocols. The fractal dimension is numerically calculated using the box-counting method by varying the size of box length e and counting the number of boxes N needed to cover all points [33]. Except for the concatenation between the [[3,1,1]] and [[4,1,1]] code, the other concatenations will give fractal dimension smaller than one.

dimensions for codes concatenated with [[15,1,3]] protocol are all smaller than one, which implies their fractal property in the one-dimensional case. For the concatenation between [[3,1,1]] and [[4,1,1]], however, the fractal dimension is very close to 1 and the distribution of fixed points might be everywhere but not dense.